JOURNAL OF CATALYSIS 152, 396–409 (1995)

Activity and Characterization of Self-Supported Model Catalysts Derived from Cobalt-Based Clusters of Clusters: Hydrogenation of 1,3-Butadiene

Miguel A. Bañares,* Laurent Dauphin,† Victor Calvo-Pérez,† Thomas P. Fehlner,† and Eduardo E. Wolf*

*Department of Chemical Engineering, University of Notre Dame, Notre Dame, Indiana 46556; and †Department of Chemistry and Biochemistry, University of Notre Dame, Notre Dame, Indiana 46556

Received July 8, 1994; revised October 24, 1994

Complex coalt–carbonyl ligand-based clusters of clusters are used as molecular precursors for self-supported model catalysts. These precursors present two metal layers. The outer layer is associated with the complex Co–carbonyl ligands, and the core layer, which is either cobalt or zinc. These two precursors are identified as CoCo and ZnCo, respectively. *In situ* DRIFTS, TGA, TPD–MS, XPS, and catalytic measurements show two distinct forms of the catalysts. Partial thermolysis at low temperature (LT) under hydrogen results in almost completely decarbonylated catalysts, which appear to posses a mainly unchanged carboxylate metal core. Complete pyrolysis at higher temperatures (HT) in hydrogen leads to a mixed metal environment. The activities of the catalysts are studied in the hydrogenation of 1,3-butadiene. The LT series show similar catalytic behavior during the hydrogenation of 1,3-butadiene. However, significantly different catalytic behavior is observed between the HT catalysts. The effect of the core metal on the *d*-electron density appears to be the factor leading to very different catalytic behavior patterns. © 1995 Academic Press, Inc.

INTRODUCTION

The use of organometallic precursors to prepare small catalyst particles is a well-known approach in catalysis (1, 2). Unfortunately these materials often lose their structure upon activation or interaction with the support (3, 4). Coordination compounds with complex cluster substituents ("clusters of clusters") present precursors for high-surface-area metal catalysts (5). Previously we reported some activity trends of materials derived from $Co_4O[(CO)_9Co_3CCO_2]_6$ and $Zn_4O[(CO)_9Co_3CCO_2]_6$ in the catalytic hydrogenation of 1,3-butadiene (6). In this paper we characterize in much more detail the new materials resulting from the cluster pyrolysis in hydrogen as well as helium. Relationships between structural features and catalytic activity for the hydrogenation of 1,3-butadiene are suggested.

EXPERIMENTAL

Catalysts' preparation. The preparative methods for the molecular precursors $Co_4O[(CO)_9Co_3CCO_2]_6$ and $Zn_4O[(CO)_9Co_3CCO_2]_6$ have been described elsewhere (5–9). These molecules have an O atom centered tetrahedral core of either cobalt or zinc atoms (Fig. 1). The six edges of the core metal tetrahedron are bridged by six cobalt carbonyl cluster carboxylate ligands. Qualitatively the structure of the molecular precursors is a layered one. The outermost layer is made up of carbonyl ligands, the second layer is cobalt metal atoms, Co(0), the third is CCO_2 moieties, and the last is the second metal (Co(II) or Zn(II)). The molecular precursors themselves show no catalytic activity in the hydrogenation of 1,3-butadiene and thermal activation is required to yield active materials. Activation is performed either under a helium, hydrogen or 1,3-butadiene/hydrogen atmosphere. Activation of the molecular precursors is carried out *in situ* prior to the activity measurements since the activated materials are readily oxidized by air. Two activation temperatures are used, 393 and 493 K. Each treatment is run for 2 h. The resulting solids are referred as CoCo and ZnCo.

Thermogravimetric analyses. The weight loss taking place for the different treatment procedures of the catalysts was measured with a Cahn RG electrobalance. The sample temperature was increased linearly from room temperature to 400°C for 190 min in flowing helium or hydrogen (100 ml/min, NPT). The electronics of the electrobalance were purged with flowing argon. All the gases used were ultra-high purity (99.999%) and, in addition, traps to remove water were incorporated into the lines. The weight loss was recorded as a function of the temperature.

Temperature-programmed decomposition-Mass spectrometry. To identify the nature of the species evolving

0021-9517/95 $6.00

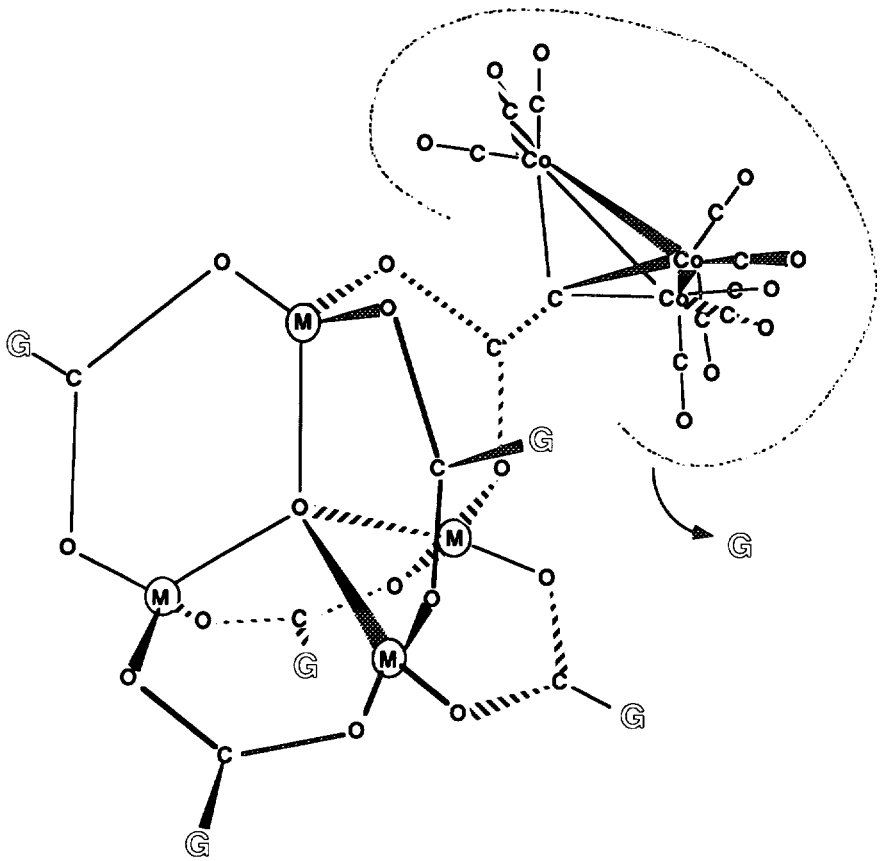

FIG. 1. Schematic drawing of the molecular structure of the Co-based clusters of clusters, M=Co, Zn.

from the molecular precursors during the activation, mass spectrometric analyses were performed with a UTI-100-C quadrupole mass spectrometer equipped with a fast response continuous inlet system. Preliminary mass scans were performed during the activation of the samples to determine all the *m/e* signals generated during the activation of the molecular precursors. *m/e* values were recorded for the analysis of CO, CO_2, CH_4, H_2O, hydrocarbons, and oxygenates C_1. The precursors were heated from 298 to 623 K for 45 min in flowing helium or hydrogen (100 ml/min). The evolution in time of the different *m/e* intensities were recorded as a function of the temperature of the sample being pyrolyzed.

Infrared studies. Information on the nature of the structure of the molecular precursors was obtained from *in situ* infrared studies. These were performed in a DRIFTS reaction cell (Harrick Co.) placed in a FTIR spectrometer (Mattson Model Galaxy-2000). As the intense absorptions associated with the carbonyl and carboxylate vibrational modes are characteristic of the outer and inner metal bonding environment, we were able to follow the structural changes of the molecular precursors during the activation in helium, hydrogen, or in the presence of the reaction mixture (hydrogen and 1,3-butadiene). For these studies ca. 5 mg of the molecular precursor was mixed with ca. 85 mg of KBr (Aldrich) and placed as a highly divided powder on the sample holder. The DRIFTS cell is designed so that the gases will flow into it from beneath the sample and through it, ensuring an appropriate contact between the gases and the catalysts. The catalyst temperature was controlled by means of a heating cartridge.

During activation of the cluster precursor a significant decrease in the volume of the sample is observed (5). Dilution in KBr minimizes this phenomenon and the reflected signal remains focused into the detector during the whole experiment. The total flow for either helium, hydrogen, or the reaction mixture (2% butadiene in hydrogen) is 50 ml/min. This was chosen in order to keep the residence time on the catalyst similar to that in the flow reactor during the catalytic experiments. All the infrared spectra are calculated in Kubelka–Munk–Shuster units (10), for a system that scatters radiation (11). Scans (416) were averaged at 4 cm^{-1} resolution. Each spectrum requires 4–5 min and the single-beam emisivity spectra are ratioed to pure KBr in equivalent conditions to correct for temperature effects. The sample is heated in steps of

10 K. The catalysts diluted in KBr show similar product selectivity but lower conversion than the undiluted catalysts in the flow micro reactor. There were no qualitative differences in the catalytic behavior of KBr mixed and KBr free materials as far as the catalytic activity was concerned.

XPS measurements. Further characterization of the molecular precursors during activation was carried out utilizing XPS. These spectra were recorded after temperature treatments of the sample under different conditions in a pretreatment chamber attached to the spectrometer. XPS measurements were conducted in a Kratos SAM-800 spectrometer using a magnesium anode. Samples in the form of thin films were prepared by evaporating a concentrated solution of the corresponding molecular precursor in THF on the surface of gold-plated copper holders. The holders were mounted on heatable insertion probe and placed in the XPS pretreatment chamber. XPS of the fresh molecular precursors were performed after evacuating the samples. Additional pretreatment was performed under flowing hydrogen in the pretreatment chamber at a pressure of 0.3 Torr while the sample was heated for 2 h at 373–423 and 473 K. Prior to any measurement, the pretreatment chamber was evacuated to 10^{-8} Torr and cooled down to room temperature. The C1*s*, O1*s*, Co2*p*, and Zn2*p* ionization regions were analyzed. The reported binding energies (BE) are referenced to a C1*s* BE of 285.0 eV.

Surface area determination. The B.E.T. surface areas were measured with a Quantachrome unit at 77 K with nitrogen as the adsorbate and helium as the carrier gas. Materials were prepared *in situ* from the appropriate precursors in order to avoid changes due to oxidation in air. The activation of the samples was performed *in situ* under flowing helium or hyrogen. The weight of the pure cluster precursor was ca. 40 mg.

Catalytic activity. The hydrogenation of 1,3-butadiene was studied in a quartz flow microreactor (4 mm i.d.) at atmospheric pressure in the temperature range 310–473 K. Typically 16 mg of the specific molecular precursor, confined with quartz wool, were activated under a hydrogen/1,3-buradiene reaction mixture with a hydrogen: butadiene = 50:1 molar ratio at a total flow rate of 100 ml/min. The proportions of hydrogen and 1,3-butadiene were changed in the reaction feed to determine the reaction order of both reactives. In these measurements helium was used to keep the total flow constant. Mass flows were controlled by electronic flow controllers (Brooks, mod. 5850-E), and the reaction system was automated and computer controlled. The reactor effluent was analyzed by gas chromatography on a Hewlett-Packard 5890-II GC provided with a FID detector. A picric acid packed column (6 ft × $\frac{1}{8}$ in.) supplied by Alltech was used to separate the effluents which were mainly 1-butene, *n*-butane, *cis*-2-butene, and *trans*-2-butene. Hydrogenolysis products produced during activation were analyzed similarly in the same column.

RESULTS

Thermogravimetric analyses. The thermogravimetric analyses during the pyrolysis of the precursors show two stages (Fig. 2). For ZnCo, the first stage of activation in helium corresponds to the loss of 37 carbonyl ligands, and the second stage to the loss of the remaining carbonyl ligands and carbon dioxide molecules moieties from the carboxylate ligands. In hydrogen the initial mass loss is less but the final mass loss is larger. The results for CoCo are very similar to those for ZnCo. The structures obtained in the first plateau under these treatments are designated as the low-temperature catalysts (LT followed by the name of the specific precursor). The catalysts resulting from treatments in the higher-temperature regime are designated as the high-temperature catalysts (HT followed by the name of the specific precursor).

Temperature-programmed decomposition–Mass spectrometry. The TPD–MS in helium of both precursors (Fig. 3) show the evolution of species with m/e at 16, 28, and 44, corresponding to CO (28) and CO_2 (16, 44). The signal for carbon monoxide is significantly higher than that for carbon dioxide. This observation is in agreement with the stoichiometry of the clusters if the carbonyl ligands evolve as carbon monoxide and the carboxylate ligands as carbon dioxide.

Pyrolysis of CoCo in helium produced significant amounts of carbon monoxide which starts to evolve at ca. 350 K (maximum at ca. 420 K) and carbon dioxide from ca. 400 K (maximum at ca. 440 K), with additional signals of lower intensity observed at ca. 580 K (Fig. 3a). Activation of CoCo in hydrogen results in the production of large amounts of carbon monoxide from ca. 320 K (maximum at ca. 420 K) and smaller amounts at ca. 490 and 520 K. The amounts of carbon dioxide evolved was significantly lower than under helium; however, additional new species can be observed at *m/e* 29 (methanol) with a maximum at ca. 420 K and at *m/e* 15 (methane) with maximum intensity in the temperature range 470–520 K. Production of water (*m/e* 18) is observed along with the evolution of methane and methanol.

Activation of ZnCo in helium shows evolution of large amounts of carbon monoxide mainly at ca. 420 K and to a lesser extent at ca. 550 K (Fig. 3b). Activation under hydrogen results in the observation of carbon monoxide from ca. 320 K until a maximum is reached at ca. 410 K. In contrast with treating in helium, no carbon dioxide is produced in H_2, but methanol (*m/e* 29) starts being

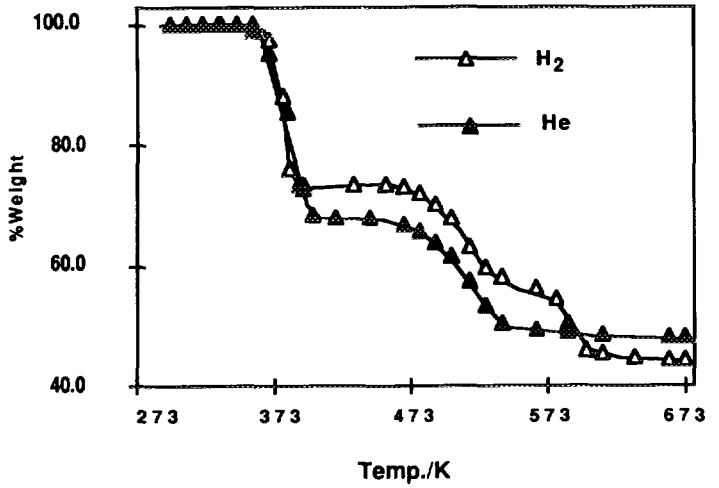

CoCo

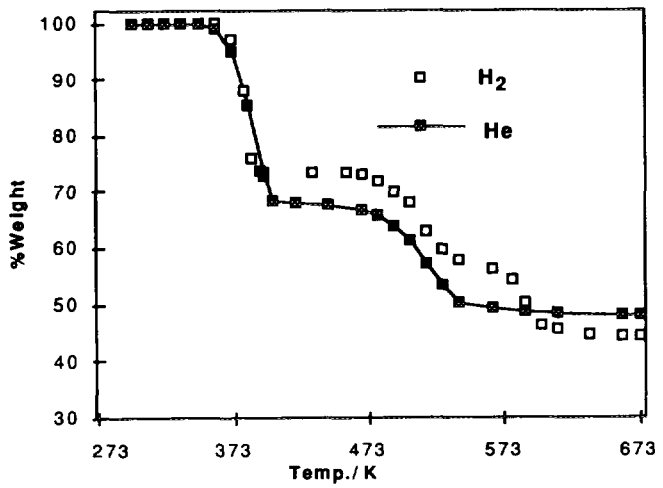

ZnCo

FIG. 2. TGA analyses of CoCo (top) and ZnCo (bottom).

produced at temperatures near 370 K (maximum at ca. 410 K). Carbon dioxide and methanol present maxima at ca. 500 and 520 K, respectively. Production of water is also significant in the range 420 to 520 K.

In situ IR of catalyst activation. The infrared spectra during the activation of the precursors CoCo and ZnCo under helium are presented in Figs. 4a and 4b. Several infrared bands are observed in the range 2110–1900 cm^{-1} characteristic of the vibrational modes of a terminal carbonyl species. The sharp bands observed at 1554 and 1387 cm^{-1} correspond to the antisymmetric and symmetric stretching vibrational modes of the carboxylate ligands, respectively (9). Heating the sample causes significant changes in the carbonyl bands. In addition a new infrared band is observed at 1860 cm^{-1} and this is assigned to the formation of bridging carbonyls (12). The appearance of bridging carbonyl is associated with the loss of terminal carbonyl ligands as gaseous CO as shown by TPD–MS analysis and TGA measurements. Loss of carbonyl ligands generates coordinatively unsaturated metal centers and sharing of carbonyl ligands by forming bridges may be a response to the formal unsaturation of the clusters.

Because of complex changes in the terminal CO stretching region, measurement of the loss of carbonyl ligands by the change in the area of the associated infrared bands is not possible. However, the well-resolved band at 2108 cm^{-1}, characteristic of the $(CO)_9Co_3CR$ cluster, can be used to estimate the relative proportion of intact clusters remaining. On heating, a continuous decrease of the infrared band at 2108 cm^{-1} is observed. The decrease of this band corresponds to the increase for the area of the infrared band at 1867 cm^{-1}. This behavior agrees well with the assignment of these bands. After the bridging carbonyl stage ends, an infrared band is still observed in the carbonyl region. This is located at ca. 1940 cm^{-1} and its

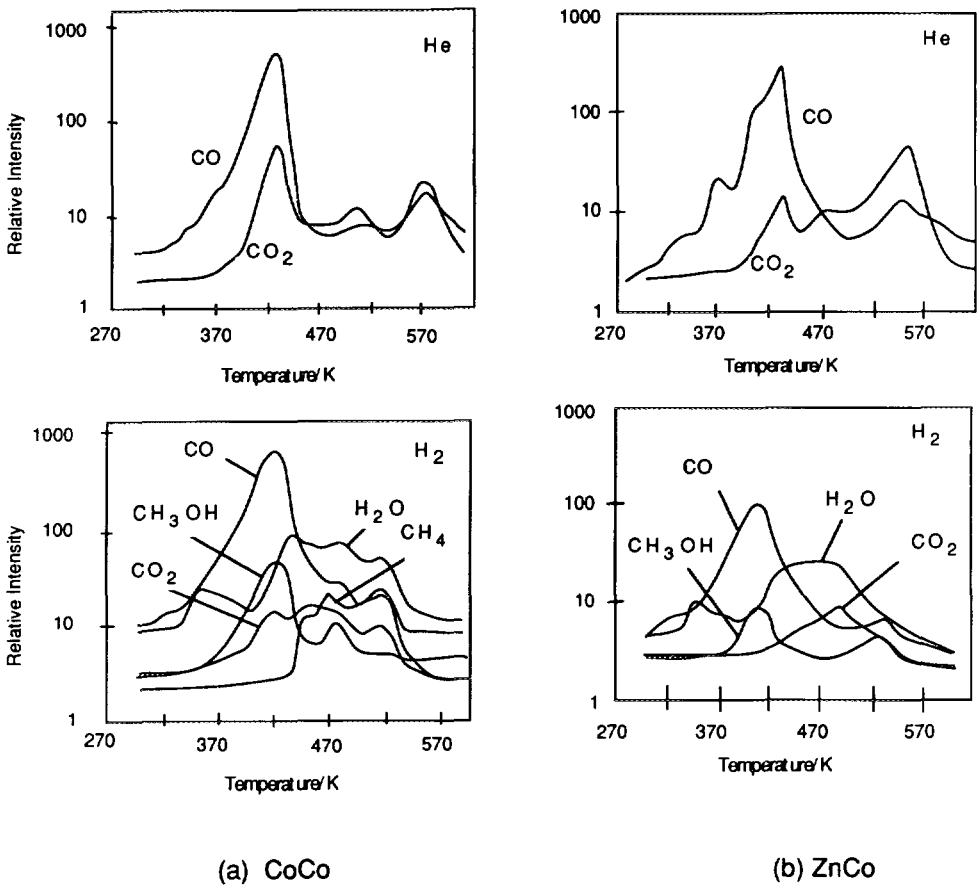

FIG. 3. TPD–MS: (a) CoCo, He (top), H_2 (bottom); (b) ZnCo, He (top), H_2 (bottom).

frequency and intensity decreases with increasing temperature. This band is reminiscent of the absorptions produced by CO adsorbed on metal particles (13). Here too there is a shift of band maximum to lower wavenumbers with decreasing coverage (13). The presence of some carbonyl species in the LT structures is in agreement with the weight loss recorded on the electrobalance, with the evolution of CO at temperatures higher than 300 K during the TPD–MS experiments, and with the presence of a weak band of oxidized carbon in the XPS measurements (see below). The loss of the coordinated carbonyl ligands from the cluster substituents is accompanied by the broadening of the infrared bands in the carboxylate region. These bands transform into two broad bands at 1560–1580 and 1440–1417 cm^{-1}. Similar bands have been assigned previously to the antisymmetric and symmetric stretching vibrations of surface acetate ions (14), and are observed here up to temperatures close to 500 K. The fact that the elimination of carbonyl and carboxylate ligands are not observed at exactly the same temperatures as in the TPD–MS measurements is attributed to the stepwise, slower heating rate during the *in situ* DRIFTS experiments. In the former case the heating rate was significantly faster (6 K/min vs steps of 10 K every 5 min) than during the infrared studies.

During activation in hydrogen (Figs. 4c and 4d) the infrared bands in the carboxylate region appear better resolved than during activation in helium and the intensity of the symmetric vibration is higher than that of the antisymmetric one. This is opposite to what is observed during activation in helium. In addition the temperature difference between the loss of carbonyl and carboxylate bands is ca. 75 K for activation in hydrogen but only ca. 25 K for activation in helium.

When the samples are activated in the presence of the reaction mixture (Figs. 4e–f), the infrared bands in the carbonyl and carboxylate regions exhibit a behavior similar to that displayed during the activation in hydrogen. An increase in the maximum intensity of the bridging carbonyl band is observed in the sequence helium, hydrogen, and hydrogen/1,3-butadiene reaction mixture. Table 1 presents some characteristics of the *in situ* infrared measurements for the cobalt-based clusters of clusters.

The more facile elimination of the carbonyl ligands compared to the carboxylate ligands suggests the existence of a partially decomposed structure supported by the car-

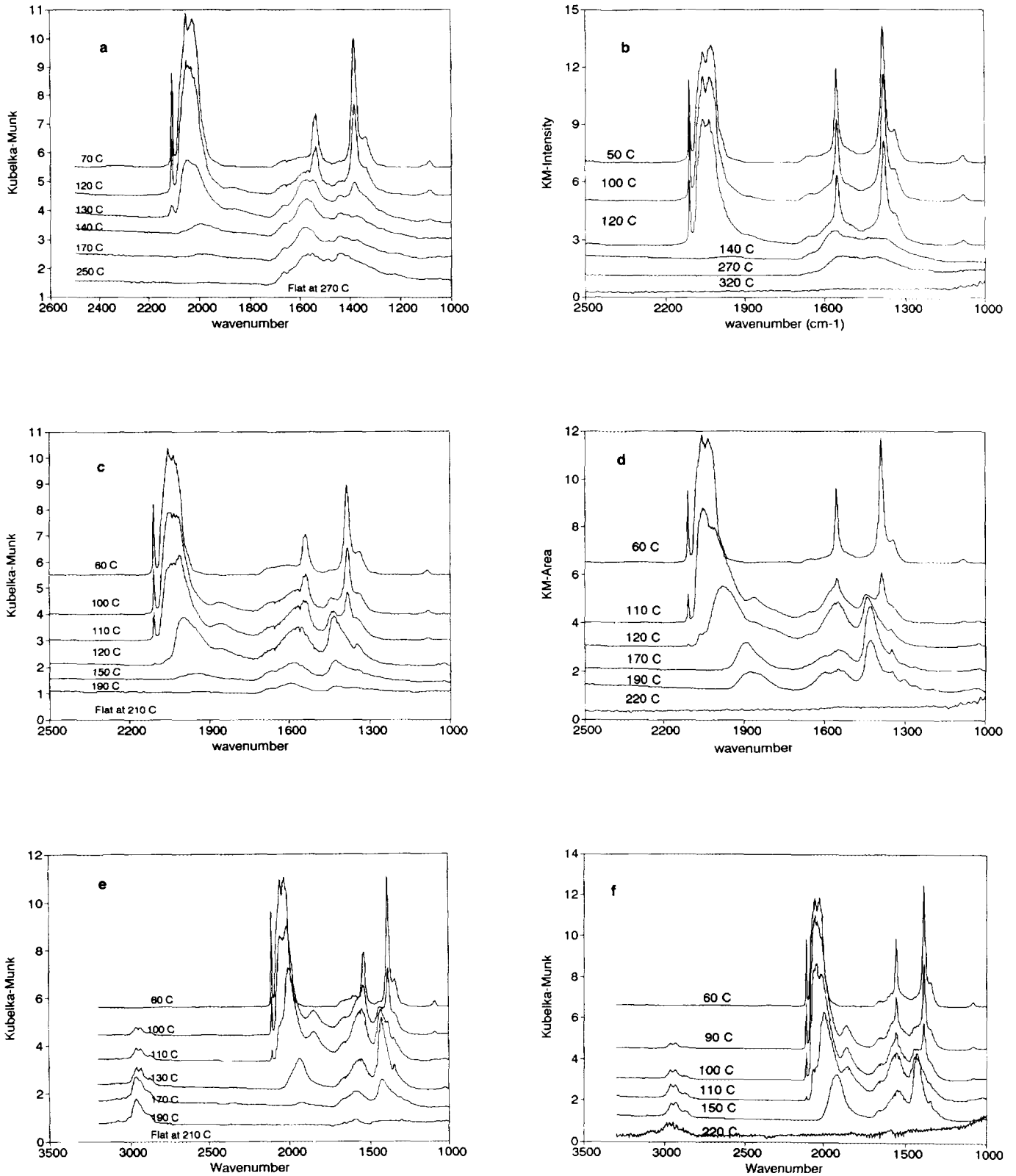

FIG. 4. *In situ* DRIFTS during activation of CoCo (left) in (a) helium; (c) hydrogen; and (e) reaction mixture (butadiene/hydrogen); of ZnCo (right) in (b) helium; (d) hydrogen; and (f) reaction mixture (butadiene/hydrogen).

TABLE 1

In situ DRIFTS Activation of the Cobalt-Based Clusters of Clusters

Precursor	Activation feed	Bridge/linear carbonyl[a]	$T_{carbonyl}$[b] (K)	$T_{carboxylate}$[b] (K)
CoCo	He	0.2	523	543
	Hydrogen	1.0	483	483
	C_4H_6/H_2	1.3	483	483
ZnCo	He	0.1	503	593
	Hydrogen	1.0	493	493
	C_4H_6/H_2	2.1	503	503

[a] Ratio of the maximum area of the infrared band at ca. 2108 cm^{-1} and the maximum area observed for the band of the bridging carbonyl species.

[b] Maximum temperature where infrared bands for carbonyl or carboxylate species are observed.

boxylate ligands. Infrared analyses were carried out on samples treated in the flowing reaction mixture at temperatures high enough to promote the elimination of the carbonyl ligands but below the temperatures where the infrared bands of the carboxylate ligands are completely removed. These treatments were performed at temperatures between 373 and 400 K, close to the maximum elimination of the carbonyl species. Infrared results show that the species holding the carboxylate ligands are stable during reaction conditions.

The surface areas of the materials are given in Table 2. Preparation under helium or hydrogen yields large surface area materials for both precursors under the low-temperature conditions. Under high-temperature conditions some loss of surface area is observed for a helium atmosphere but for preparations under hydrogen the area loss is much more substantial. Presumably, then, under the reaction conditions the relevant surface areas are those measured for materials prepared in a hydrogen atmosphere.

In situ IR of 1,3-butadiene hydrogenation. The alkyl species adsorbed on the catalysts during 1,3-butadiene hydrogenation reaction were studied in the DRIFTS reaction cell. During activation in the reaction mixture, additional infrared bands are observed near 2965, 2935, 2877, and 2862 cm^{-1}, which are characteristic of aliphatic C–H vibrations (15–17). The group assignments for the vibrational groups are given in Table 3. The intensities for the symmetric vibrational mode bands are significantly lower than those of the asymmetric vibrational modes. The bands for the symmetric C–H vibrational modes for the methyl and methylene groups are observed as two broad features, and little information can be obtained from them. However, the infrared bands located near 2965 and 2935 cm^{-1} (antisymmetric C–H vibrational modes of the methyl and methylene groups) are clearly observed and their intensities can be measured. Discussion of the significance of these bands is presented below.

TABLE 2

BET Surface Area (m^2/g)

	CoCo		ZnCo	
Treatment	Helium	Hydrogen	Helium	Hydrogen
373 K/2 h	160	193	280	350
473 K/2 h	52	2	200	50

TABLE 3

Group Assignments of the C–H Infrared Bands

Group	Mode	Frequency (cm^{-1})
CH_3	n_{as}	2965
	n_{sy}	2877
CH_2	n_{as}	2935
	n_{sy}	2860

In situ XPS. The *in situ* XPS measurements after the activation of CoCo and ZnCo in vacuum are presented in Fig. 5 for the precursor (a), after heating at 373 K (b), and at 473 K (c). The C1*s* binding energy of all catalysts show a band at 285.0 eV, corresponding to adventitious carbon which is used as a reference to correct the charging effects on the samples during the analyses. It is interesting to remark that the extent of charging in the samples decreased as the extent of activation increased. This is indicative of the metallic character of the final product. In addition to this carbon band, another band can be observed at 288.2 eV, characteristic of carbon in carbonyl or carboxylate ligands. During activation the binding energy of Co2*p* shifts from 780 eV to 778 eV, indicative of reduction from coordinated cobalt (II) to metallic cobalt. In the case of CoCo, partially activated samples (393 or 493 K) show a weak band at 780 eV. This band is associated with the core cobalt atoms, which are still coordinated to the carboxylate ligands. The binding energy region of Zn2*p* from ZnCo precursor does not show significant shift during the activation, as expected, since the binding energy of Zn2*p* is not very sensitive to the chemical environment (18). The relative intensities of Co2*p* and Zn2*p* (Table 4) show a change during the activation of the samples. An initial increase of all the metal signals are observed for samples treated at 393 or 493 K, mainly due to the elimination of the carbonyl ligands from the outermost layer. However, activation of ZnCo at 573 K results in a important decrease of the intensity of Co2*p*, which, along with a smooth increase of the Zn2*p* intensity, indicates a rearrangement in which Zn migrates to the surface. XPS results indicate enrichment of surface by Zn

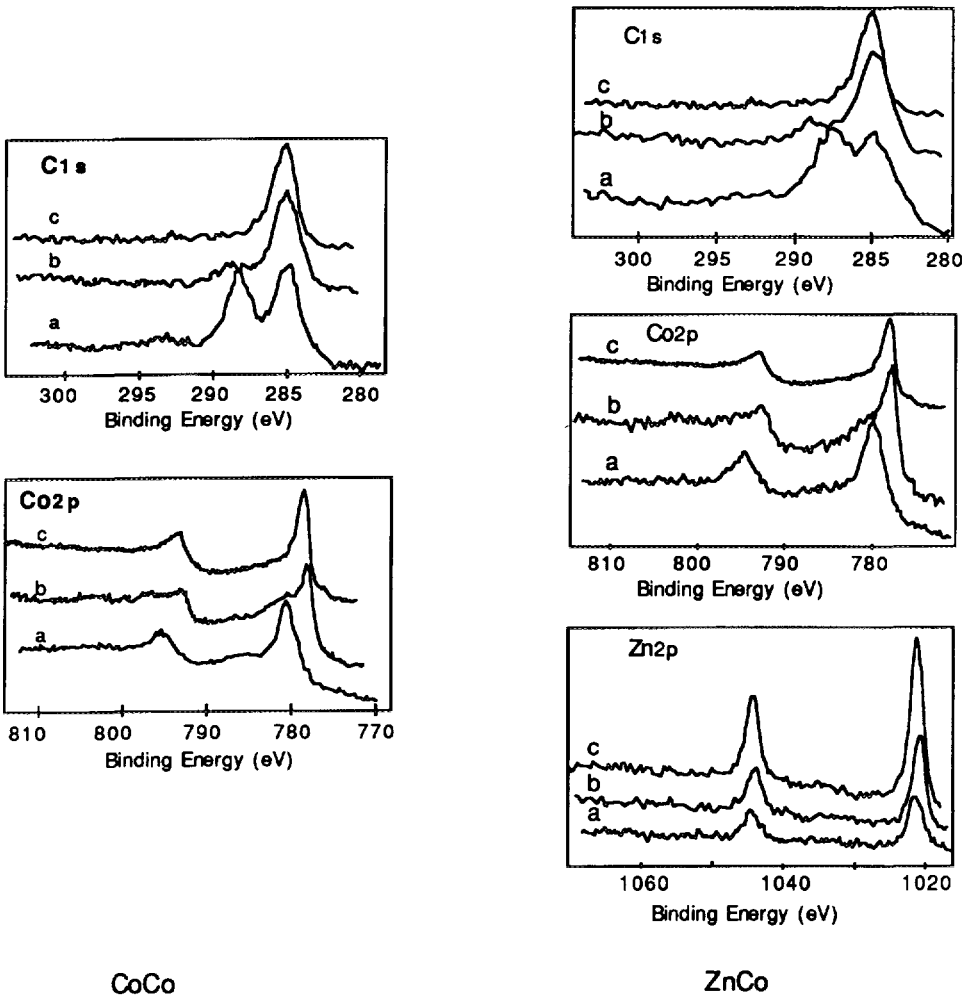

FIG. 5. XPS: CoCo (left); C1*s*, and Co2*p*; ZnCo (right); C1*s*, Co2*p*, and Zn2p. In each case (a) is the spectrum of the precursor, (b) the spectrum after heating at 373 K, and (c) the spectrum after heating at 473 K.

at the higher-activation temperatures. This has to occur by solid–solid diffusion of zinc toward the surface through a cobalt layer. Shift in the binding energy indicates reduction to metallic state or metallic bonding. However, the difference between these two cases cannot be ascertained. As demonstrated previously, no significant differences in the XPS were observed after treatment under the hydrogen/butadiene reaction mixture (6).

TABLE 4

Relative XPS Areas During Pyrolysis of ZnCo

Sample	Co2p	Zn2p
Fresh	85.9	46.1
120°C	102.0	74.9
220°C	95.4	18.5
300°C	61.8	128.5

Hydrogenation of 1,3-butadiene. The hydrogenation of 1,3-butadiene yields mainly 1-butene, butane, *trans*-2-butene, and *cis*-2-butene. Trace amounts of $C_{<4}$ are also obtained, which in the case of HT CoCo became significant. Hydrogenation is observed starting at room temperature. A blank test using only quartz wool revealed conversions of butadiene of 7 and 20% at 373 and 473 K, respectively, where 1-butene was the main product formed. Table 5 shows temperatures for 50% conversions and Figs. 6a and 6b show the selectivity–conversion trends for the LT CoCo and ZnCo catalysts. The turnover frequencies (TOFs) were found to be in the range 10^{11}–10^{14} molecules/s cm^2 of catalyst surface area. At low conversions, 1-butene is the main hydrogenation product. An increase in the conversion results in an increase in the selectivity for butane which at conversions above ≈80% becomes the main hydrogenation product. The selectivities for 1-butene and *n*-butane are complementary. However, the selectivities for 2-butenes are independent of the

TABLE 5

Temperature (K) for 50% Conversion

Structure	CoCo	ZnCo
LT	324	345
HT	313	371

Note. Reaction conditions: Hydrogen/1,3-butadiene, 50/1; flow, 100 ml/min; and *W* precursor, 16 mg.

extent of 1,3-butadiene conversion and the accompanying changes in selectivity to *n*-butane and 1-butene. Similar behavior is observed for all the LT catalysts.

The catalytic behavior differs markedly among the different samples in the HT series. HT CoCo is selective for full hydrogenation (*n*-butane) even at very low conversion levels. Hydrogenolysis products are obtained for this catalyst in a higher amount than the rest of the HT series. Conversely, the bimetallic ZnCo catalyst shows a higher selectivity to partial hydrogenation (mainly 1-butene). For the HT catalyst the presence of Zn appears to affect the chemistry of the reaction preventing the complete hydrogenation to butane. This is true even at temperatures 50 K higher than those required to obtain 100% conversion of 1,3-butadiene, whereas for the LT catalysts the presence of a second metal has no significant effect on the product distribution. In all cases, selectivities to *trans*-2-butene and *cis*-2-butene did not surpass ca. 25 and 15% selectivity, respectively, and their selectivities do not appear to be affected by the relative formation of *n*-butane or 1-butene.

The reaction order for hydrogen was always near one and it was near zero for butadiene. Similar results have been obtained in other catalytic systems for the same reaction (19, 20) and this strongly suggests that under the reaction conditions the surface is saturated with the adsorbed hydrocarbon.

DISCUSSION

Catalyst activation. Thermal activation of the different precursors results in an initial loss of carbonyl ligands,

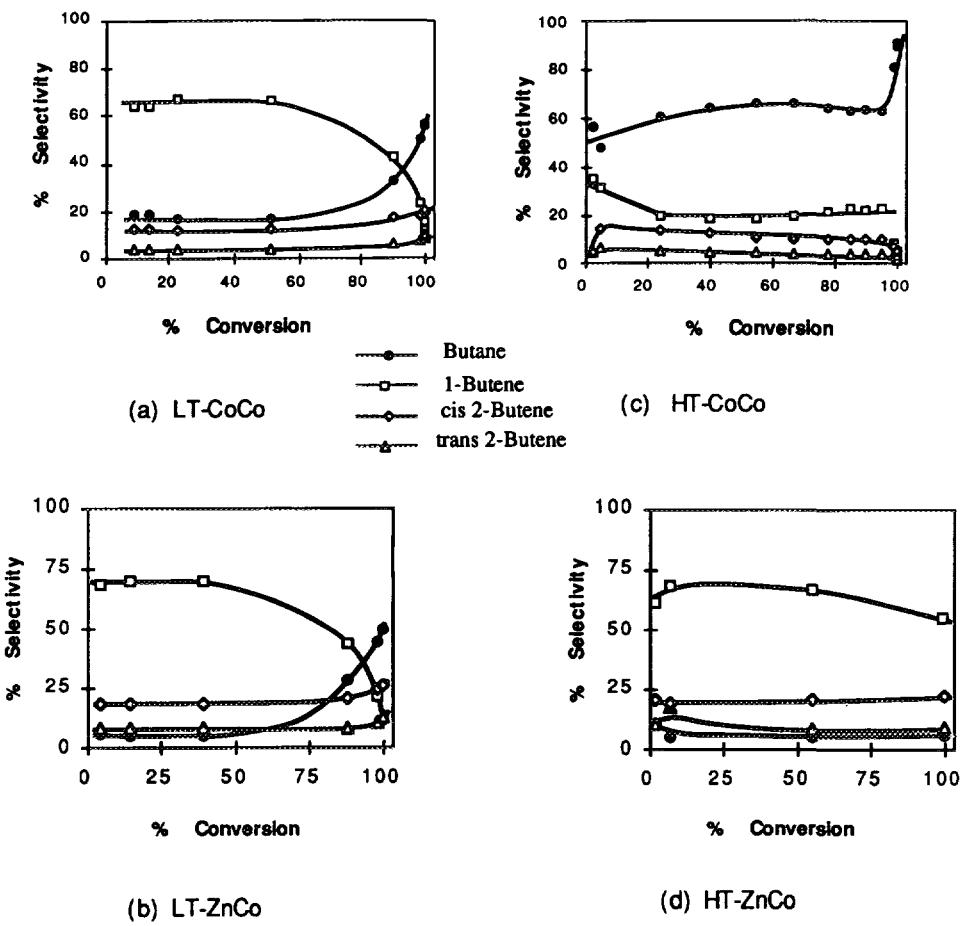

FIG. 6. Selectivity vs butadiene conversion. (a) LT-CoCo; (b) LT-ZnCo, (c) HT-CoCo, (d) HT-ZnCo; Reaction feed, 100 + 2 ml/min 1,3-butadiene + Hydrogen.

while further heating results in the elimination of the carboxylate ligands. The temperature gap between the total loss of the carbonyl and carboxylate ligands allows the formation a partially decomposed species, the low temperature catalysts, resulting from the loss of most carbonyl ligands. While there is no direct evidence of the geometrical structure, the IR and the TGA results point to the carbonyls leaving first, then the carboxylates which would leave the core structure intact. The presence of the carboxylate ligands suggests that the core structure in the LT species is similar to that observed for the initial precursors (Fig. 1). Consequently, the LT series may consist of a metal–carboxylate core structure covered by cobalt atoms. The shrinkage of the structures (5) will create pores with internal surfaces of cobalt atoms independently of the presence of Co or Zn within the cluster core. The relative arrangement of the metal atoms appears to be mostly retained (Fig. 7). The inner cobalt atoms are screened from each other structurally and electronically by carboxylate groups in LT catalysts. Hence only outer cobalt atoms should be catalytically active.

Further activation of the LT structures at higher temperatures (HT activation) results in elimination of the remaining carbonyl ligands and of the carboxylate ligands as supported the infrared, TGA, and TPD–MS measurements. This elimination, however, requires the presence of hydrogen to be complete at lower temperatures. TPD–MS experiments show that carbonyl species are removed as carbon dioxide under helium. The use of hydrogen instead of helium promotes the activation of the clusters due to the reaction with the carboxylate ligands to yield methane or oxygenates-C_1 and water. It is interesting to note that acetate species are also observed during the hydrogenation of carbon monoxide (14). The formation of methane and water from CoCo or oxygenates-C1 and water from ZnCo and the fact that cobalt-based catalysts are used in Fischer–Tropsch reactions may account for the easier elimination of these species under hydrogen, since a chemical reaction is the driving force to remove the carboxylate ligands. The different reactivity of the species resulting from the different molecular precursors is also reflected here since methane is produced in CoCo, whereas ZnCo, which is less reactive to complete hydrogenation, yields mainly methanol.

Activation in the reaction mixture yields a behavior similar to that in hydrogen; however, the transient formation of bridging carbonyl species appears to be further enhanced (Fig. 4). Again, during the first stages of the reaction, in addition to the hydrogenation of the ligands already discussed, butadiene molecules adsorb and react. The *in situ* infrared spectra provide evidence for the presence of adsorbed hydrocarbon species. The selectivity of the fresh or partially pyrolyzed cluster is essentially toward olefins and, as decarbonylation proceeds, activity and selectivity values tend to those of the LT catalysts. Even though the structures formed during the activation of the LT catalysts are not stable, *in situ* infrared spectroscopy provides additional information on the structure and activity of the catalysts at this stage.

The selectivity trends analyzed from the effluents of the DRIFTS reaction cell during the activation of the precursors at low temperature (373 to 423 K) in the reaction mixture show that 1-butene is the main hydrogenation product as long as significant amounts of carbonyl ligands are still present on the precursor. After elimination of these species, weaker carbonyl bands at ca. 1940 cm^{-1} associated with adsorbed carbonyl are observed. The slow continuous elimination of these adsorbed species results in a continuous increase for the selectivity for complete hydrogenation. The time required for the switch in selectivity (1-butene to *n*-butane) during the initial decarbonylation of the clusters decreases with increasing activation temperatures and is always associated with the elimination of the bridging carbonyl species. If this treatment is performed at higher temperature (473 K), complete decarbonylation takes place readily and the activity observed even at early stages is much closer to the activity of the fully pyrolyzed material. For the representative CoCo precursor activated at 373, 423, and 473 K in reaction mixture, ca. 200, 80, and less than 10 min, respectively, are required for a switch in selectivity trends (1-butene to *n*-butane). Very similar transient behavior is

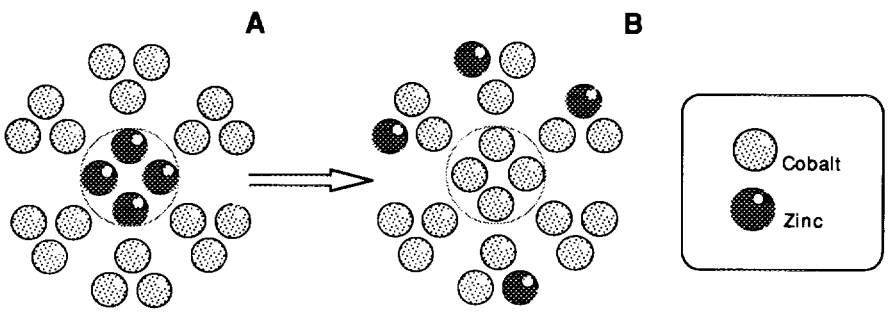

FIG. 7. Suggested relative arrangements of the metal atoms in ZnCo; (a) LT catalysts and (b) HT catalysts.

observed for the molecular precursor ZnCo during activation in the reaction mixture for different temperatures. In short, in the initial stages the catalyst activity is not significantly affected by the core metal.

Hydrogenation of 1,3-butadiene. The specific characteristics of each cluster and the method of activation used affect its catalytic behavior. The LT series presents a cobalt-like external surface still bonded to some carbon atoms, whereas on the HT series, a mixed metal surface is present. Table 5 shows the temperature required to accomplish 50% conversion on the various catalysts used, and the differences between the LT catalysts are significantly smaller than between the HT catalysts. The lower temperature required by LT CoCo to yield 50% conversion (DT ~20 K), despite its lower surface area as compared to LT ZnCo, indicates that the number of active sites do not correlate directly with the activity of these catalysts. However, the nature of the active site does not appear to be significantly affected since the selectivity trends are very close for both LT catalysts. The selectivity for *n*-butane and 1-butene show complementary trends for the LT catalysts. The selectivity ratios 1-butene/*n*-butane are higher or close to unity and at conversions above ca. 80% butane becomes the most important hydrogenation product. Most of the experiments for the LT samples were run at significantly lower temperatures (typically 313–373 K) in order to preserve the LT structure. During LT activation, the second metal not only stays in the inner layer but also no direct metal–metal bonding exists between the exposed cobalt and the core metal atoms. The bonding between the two metal layers is through the carboxylate ligand which can attenuate any electronic effects from the second metal.

Conversely, significant differences are observed for the butadiene hydrogenation activity when carboxylate ligands are removed from the catalyst structure. HT ZnCo is significantly less reactive, as evidenced by the additional 60 K required to accomplish the same conversion than its homologue HT CoCo. The selectivity trends also show a profound change in the nature of the catalysts as complete hydrogenation to butane as the main product is prevented on the HT ZnCo. Meanwhile, HT CoCo not only shows a higher activity but it also shows a remarkable selectivity to butanes, even at very low conversion levels of 1,3-butadiene. The presence of Zn in the HT structure results in a catalyst highly selective to partial hydrogenation, mainly 1-butene.

The main difference between the HT and LT structures is the elimination of the carboxylate moieties. In the absence of carboxylate ligands the metals will tend to arrange according to their specific characteristics. The higher surface tension for zinc promotes its migration to the surface as the XPS analysis suggests. Consequently, the second metal is also exposed to the absorbing butadiene.

The presence of electron donors is reported to increase the selectivity to partial hydrogenation (21) as is the case of nitrogen bases (2, 22, 23) by decreasing the strength of the hydrocarbon adsorption. Zn has a higher number of *d*-electrons than cobalt and this electronic effect may account for the significant increase in the selectivity to partial hydrogenation. In fact, the presence of Zn totally prevents the formation of *n*-butane as the main hydrogenation product. The formation of *n*-butane is not accomplished even at 50 K above the temperature required to accomplish 100% conversion of 1,3-butadiene. Consequently, depending on the core metal used, we can produce a highly active catalyst for complete hydrogenation (HT CoCo) or a catalyst with a high selectivity to partial hydrogenation (mainly 1-butene) at 100% conversion of 1,3-butadiene (HT ZnCo).

Additionally, for the HT CoCo catalyst, a certain amount of hydrogenolysis was observed. This indicates the possibility of a stronger interaction with the hydrocarbon for this catalyst. The fact that the hydrogenation of 1,3-butadiene with LT CoCo occurs at a lower temperature than with HT CoCo supports the existence of a stronger interaction. Such an interaction will increase the ratio between the rate of hydrogenation to the rate of desorption, promoting the complete hydrogenation, even at low conversion of 1,3-butadiene. The infrared measurements strongly support a different interaction for the adsorbed hydrocarbon on HT CoCo, as a linear correlation observed between the relative intensities of the asymmetric methyl and methylene vibrations is not observed. The existence of a reaction pathway different than that of the LT series and the other HT catalyst is supported by the high selectivity to butane at any conversion level, the apparent activation energy of HT CoCo roughly double to that of HT ZnCo, and the formation of hydrogenolysis products on HT CoCo.

Further information on the reaction can be obtained from the nature of the hydrocarbon species adsorbed on the surface of the catalysts from IR spectroscopy. For both catalysts the reaction order for 1,3-butadiene is zero. Consequently, the surface must be saturated with adsorbed hydrocarbons (19, 20).

Figure 8 shows the most intense infrared bands observed near 2965 and 2935 cm^{-1} during the hydrogenation of 1,3-butadiene. The ratios of the intensity of the methyl and methylene group asymmetric to symmetric vibrational modes for liquid alkanes are 2.3 and 1.7, respectively (24). According to surface selection rules the intensities of modes with a dipole moment perpendicular to the surface will be enhanced (25). The $n_{as}(CH_3)/n_{sy}(CH_3)$

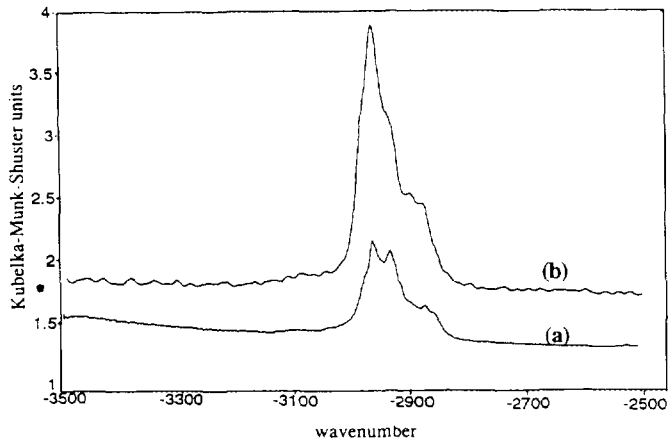

FIG. 8. Representative infrared bands of aliphatic C–H modes during reaction.

ratio were close or higher (2.3–3.0) than those expected from liquid alkanes ratios. The $n_{as}(CH_2)/n_{sy}(CH_2)$ ratios were also higher than expected (2.4–3.1). The enhancement of the asymmetric methyl and methylene modes implies that the C_{3v} axis of the methyl groups is not perpendicular to the surface (25). For the methylene group the C_{2v} axis will also be closer to parallel than perpendicular to the surface. Several structures have been proposed for the surface adsorbed butane species as shown in Fig. 9. 2,3-dimetallabutane and 1,1,2-trimetallabutane surface species have methyl groups pointing away from the surface. This should result in an enhancement of the symmetric methyl mode vs the asymmetric one, which is not the observed trend in the present case. Consequently, the 1,1,2-trimetallabutane and 2,3-dimetallabutane are probably not the predominant species on the surface of these catalysts.

The 1,1,3-trimetallabutane presents a C_{2v} symmetry axis of the methylene groups mainly parallel to the surface; consequently, its symmetric dipole moment will be parallel to the surface and its asymmetric dipole moment will be perpendicular to the surface. This may account for the significant increase of the $n_{as}(CH_2)/n_{sy}(CH_2)$ ratio. An increase of the asymmetric mode is observed with increasing selectivity to partial hydrogenation product, 1-butene. This suggests that the 1,1,3-trimetallabutane species results in the 1-butenes. Increasing selectivity to *n*-butane is associated with an increase of the intensity of

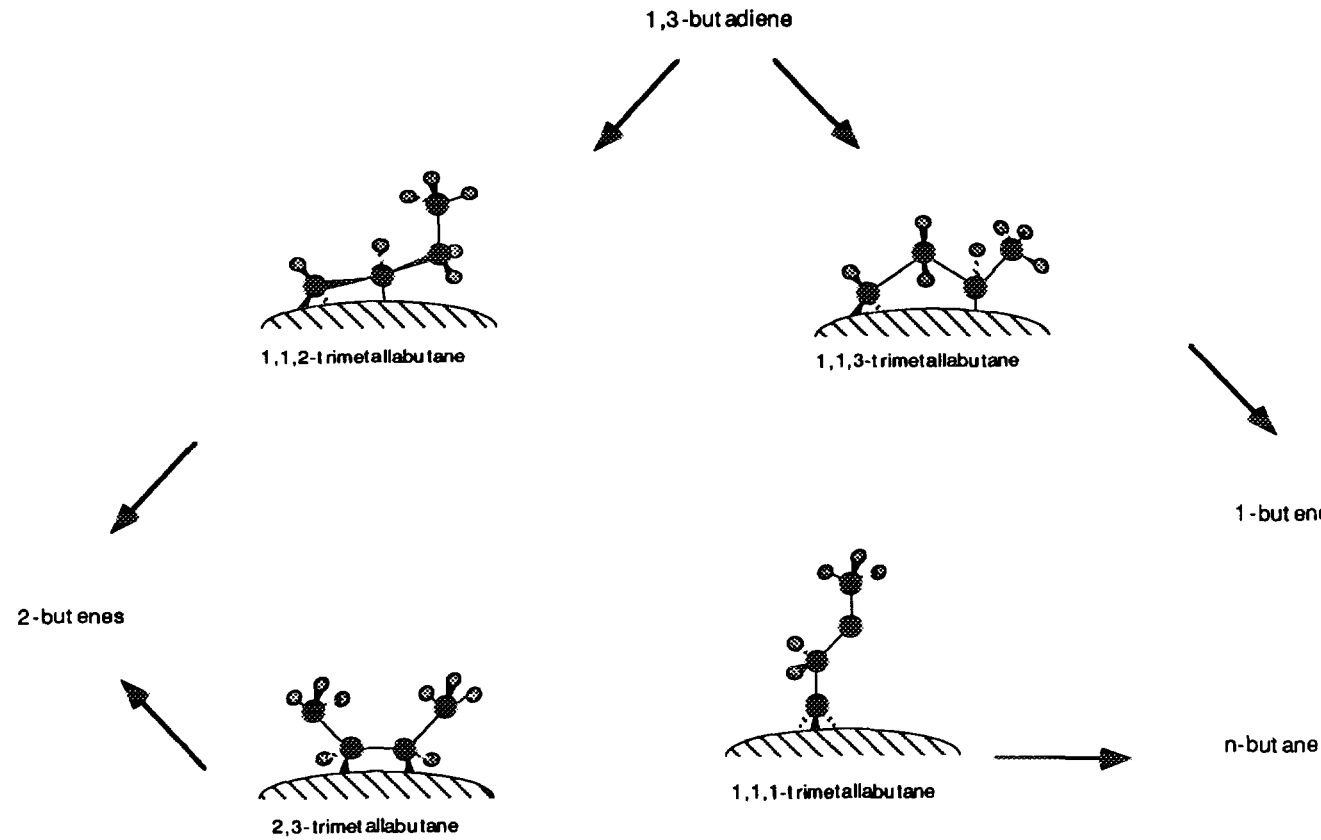

FIG. 9. Proposed surface adsorbed C_4 species.

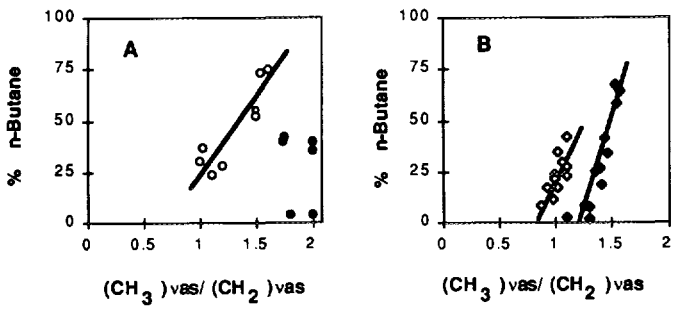

FIG. 10. $n_{as}(CH_3)/n_{as}(CH_2)$ modes intensity ratios vs selectivity to butane. (a) CoCo; (b) ZnCo. The open symbols refer to the LT catalysts and the closed symbols to the HT catalysts.

the asymmetric vibrational mode of methyl groups vs the intensity of the asymmetric mode of methylene groups. It has been proposed that the presence of alkyl-like surface species (butylidine) will increase the $n_{as}(CH_3)$ intensity since it no longer is held so rigidly to the surface with its dipole moment mainly parallel to the surface (17, 26, 27). In addition $n_{as}(CH_2)$ for the β-carbon should be attenuated. A close relation is observed between the increase of the $n_{as}(CH_3)/n_{as}(CH_2)$ and the selectivity to butane (Fig. 10). The trends observed in Fig. 10 suggest that the alkyl-like surface species may result in the formation of butane. Note that HT CoCo does not show this relation. It is interesting to remember that for HT CoCo $C_{<4}$ hydrocarbons were also observed. Consequently, the interaction of the hydrocarbons with HT CoCo may be different. Adsorbed hydrocarbons with less than four carbon atoms have to be considered. At present, no definitive analysis can be provided concerning the nature of the adsorbed hydrocarbon on HT CoCo.

The complementary selectivities between *n*-butane and 1-butene show that *n*-butane results from the hydrogenation of 1-butene. The 2-butenes must result from a different surface species since there is no connection between the trends to *n*-butane and 1-butene with those of the 2-butenes. The 2-butenes are a lower fraction of the formed hydrocarbon; consequently, the intermediates on the surface to which they are mechanistically related should not be much more abundant. The 2,3-dimetallabutane and/or 1,1,2-trimetallabutane may be the intermediate species in the formation of the 2-butenes. The presence of these species accounts for the presence of the $n_{as}(CH_3)$ mode when selectivity to butane is very low (Fig. 10).

In summary, the infrared measurements during the hydrogenation of 1,3-butadiene suggest that 2,3-dimetallabutane and/or 1,1,3-trimetallabutane species yield the 2-butenes. The 1,1,3-trimetallabutane results in the formation of 1-butene. At higher conversions, this last surface species appears to transform into an alkyl-like surface species which results in *n*-butane.

CONCLUSIONS

1. The activity of the cluster derived model catalysts can be tailored by the extent of pyrolysis of the precursor and the nature of the core metal.
2. In the LT structure the carboxylate moieties hold the environment of the core metal in an arrangement close to the one observed in the fresh clusters.
3. For the LT catalysts the core metal does not appear to have a significant effect on the hydrogenation of 1,3-butadiene since it is hindered by the external layers of carboxylate ligands and cobalt atoms. In this structure the outside cobalt metal appears to determine the catalytic behavior.
4. In the HT structure a major structural rearrangement takes place since Zn appears to enrich the surface of the catalyst and its presence on the surface exerts a significant effect on the activity of the system, most likely due to the electronic effects.
5. The formation of 2-butenes appears to result from intermediates other than 1-butene and *n*-butane. 2,3-dimetallabutane surface species and/or 1,1,2-trimetallabutane surface species appear to be responsible for the formation of the 2-butenes.
6. 1,1,3-trimetallabutane surface species result in the formation of 1-butene. Increase in the conversion appears to transform it into alkyl-like surface species that yields *n*-butane.
7. The presence of Zn in the completely pyrolyzed material prevents the complete hydrogenation to butane as the main hydrogenation product, resulting in a catalyst selective for partial hydrogenation. On the other hand, HT CoCo is an extremely active catalyst.

ACKNOWLEDGMENTS

The present work was supported by the National Science Foundation CHE91-06933. The authors gratefully acknowledge Mr. Patrick Pinhero for his aid with the XPS experiments.

REFERENCES

1. Gates, B. C., *in* "Clusters in Catalysis" (Gates *et al.*, Eds.), Elsevier, New York, 1986.
2. Iwasawa, Y., "Tailored Metal Catalysts," Reidel, Dordrecht, 1986.
3. Primet, M., El Azahar, M., and Guenin, M., *Appl. Catal.* **58,** 241 (1993).
4. Tardy, B., Noupac, C., Leclerk, C., Bertolini, J. C., Hoareau, A., Treilleux, M., Fanre, J. P., and Nohoul, G., *J. Catal.* **129,** 1 (1991).
5. Cen, W., Ladna, B., Fehlner, T. P., Miller, A. E., and Yue, D., *J. Organomet. Chem.* **449,** 19 (1993).
6. Kalenik, Z., Ladna, B., Wolf, E. E., and Fehlner, T. P., *Chem. Mater.* **5,** 1247 (1993).
7. Cen, W., Haller, K. W., and Fehlner, T. P., *Inorg. Chem.* **30,** 3120 (1991).

8. Cen, W., Haller, K. W., and Fehlner, T. P., *Inorg. Chem.* **31,** 2072 (1992).
9. Cen, W., Haller, K. W., and Fehlner, T. P., *Inorg. Chem.* **32,** 995 (1993).
10. Kubelka, P., *J. Opt. Soc. Am.* **38,** 448 (1948).
11. Klier, K., "Vibrational Spectroscopy for Adsorbed Species, ACS Symp. Ser. 137." (M. J. Comstrock, Ed.), Chap. 8. Washington, 1980.
12. Colthup, N. B., Daly, L. H., and Wiberley, S. E., "Introduction to Infrared and Raman Spectroscopy" 3rd ed., Academic Press, New York, 1990.
13. Gates, B. C., Guczi, L., and Knozinger, H., Eds. *Stud. Surf. Sci. Catal.* **29** (1986).
14. Underwood, R. P., Bell, A. T., *J. Catal.* **109,** 61 (1988).
15. Morrow, B. A., and Sheppard, N., *Proc. Royal Soc. London Ser. A* **311,** 415 (1969).
16. Campione, T. J., and Ekerdt, J. G., *J. Catal.* **102,** 64 (1986).
17. Anderson, K. G., and Ekerdt, J. G., *J. Catal.* **116,** 556 (1989).
18. Briggs, D., Seah, M. P., "Practical Surface Analysis," p. 607. Wiley, New York, 1990.
19. Pradier, C. M., Margot, E., Berthier, Y., and Oudar, J., *Appl. Catal.* **43,** 177 (1988).
20. Pradier, C. M., and Berthier, Y., *J. Catal.* **129,** 356 (1991).
21. Sarkany, A., Zsoldos, Z., Furlong, B., Hightower, J. W., and Guczi, L., *J. Catal.* **141,** 566 (1993).
22. Boitiaux, J. P., Cosyns, J., and Martino, G., "Metal Supported and Metal Additive Effects in Catalysis" (B. Imelik *et al.*, Eds.) p. 335. Elsevier, Amsterdam, 1982.
23. Boitiaux, J. P., Cosyns, J., and Vasudevan, S., *Appl. Catal.* **15,** 317 (1985).
24. Jones, R. N., *Spectrochim. Acta* **9,** 235 (1957).
25. Greenler, R. G., Snider, D. R., Witt, D., and Sorbello, R. S., *Surf. Sci.* **118,** 415 (1982).
26. Koestner, R. J., Frost, J. C., Stair, P. C., Van Hove, M. A., and Somorjai, G. A., *Surf. Sci.* **116,** 85 (1982).
27. Koestner, R. J., Van Hove, M. A., and Somorjai, G. A., *J. Phys. Chem.* **87,** 203 (1983).